ASTER Preflight and Inflight Calibration and the Validation of Level 2 Products

K. Thome, K. Arai, Simon Hook, H. Kieffer, Harold Lang, Tsuneo Matsunaga, A. Ono, F. Palluconi, H. Sakuma, P. Slater, T. Takashima, H. Tonooka, S. Tsuchida, Ronald M. Welch, and E. Zalewski

***Abstract*— This paper describes the preflight and inflight calibration approaches used for the Advanced Spaceborne Thermal Emission and Reflection Radiometer (ASTER). The system is a multispectral, high-spatial resolution sensor on the Earth Observing System's (EOS)-AM1 platform. Preflight calibration of ASTER uses well-characterized sources to provide calibration and preflight round-robin exercises to understand biases between the calibration sources of ASTER and other EOS sensors. These round-robins rely on well-characterized, ultra-stable radiometers. An experiment held in Yokohama, Japan, showed that the output from the source used for the visible and near-infrared (VNIR) subsystem of ASTER may be underestimated by 1.5%, but this is still within the 4% specification for the absolute, radiometric calibration of these bands. Inflight calibration will rely on vicarious techniques and onboard blackbodies and lamps. Vicarious techniques include ground-reference methods using desert and water sites. A recent joint field campaign gives confidence that these methods currently provide absolute calibration to better than 5%, and indications are that uncertainties less than the required 4% should be achievable at launch. The EOS-AM1 platform will also provide a spacecraft maneuver that will allow ASTER to see the moon, allowing further characterization of the sensor. A method for combining the results of these independent calibration results is presented. The paper also describes the plans for validating the Level 2 data products from ASTER. These plans rely heavily upon field campaigns using methods similar to those used for the ground-reference, vicarious calibration methods.**

***Index Terms*— Advanced Spaceborne Thermal Emission and Reflection Radiometer (ASTER), algorithm validation, geometric calibration, radiometric calibration, vicarious calibration.**

I. Introduction

THE ADVANCED Spaceborne Thermal Emission and Reflection Radiometer (ASTER) is a high-spatial resolution imaging spectroradiometer provided by the Japanese Ministry of International Trade and Industry to the National Aeronautic and Space Administration (NASA). It is part of NASA's Office of Earth Science (OES), Earth Observing System (EOS)-AM1 spacecraft [1], [2]. We include a short description of the sensor here for reference, especially those parts relevant to calibration and validation, but details on the design and operation of ASTER can be found elsewhere [3]–[5].

The sensor consists of three subsystems: the visible and near-infrared (VNIR) with 15-m resolution, the shortwave infrared (SWIR) with 30-m resolution, and the thermal infrared (TIR) with 90-m resolution [6], [7]. The details on the bands and radiometric requirements for ASTER are shown in Table I. The band 3N refers to the nadir-looking band, while 3B refers to an identical band with a separate telescope viewing in the aft direction for stereo imaging. The 0.3-K radiometric resolution for bands 10–14 are for high-radiance inputs. At low radiance, the specification is 1.5 K for bands 10–12 and 2.5 K for bands 13 and 14. The swath width for the three systems is 60 km, with cross-track pointing of 8.6° for the SWIR and TIR subsystems and 24.0° for the VNIR subsystem.

The VNIR system consists of an 80-mm diameter primary mirror for both nadir and backward-looking telescopes. The design uses compensation lenses to provide higher optical performance [8], and a 5000-element, linear-array charge coupled device (CCD) of silicon photodiodes produces the cross-track coverage. Beam splitters create three light paths to three separate interference filter/CCD pairs located on the same focal plane. A single array is used for the backward-looking radiometer. Rotating both telescopes with a stepper motor gives the cross-track pointing.

The SWIR system consists of a 190-mm diameter lens system [9]. 2048-element platinum silicide arrays of Schottky barrier photodiodes provide cross-track coverage. Six pairs of staggered linear CCD arrays are located on a single chip. The spectral bands are defined by interference filters in front each array pair. The design of the VNIR system is such that it samples a location on the ground with all three arrays simultaneously. However, the width of the interference filters for the SWIR bands requires a downtrack spacing that causes up to a 12.3 km offset between bands on the ground. A rotating, flat mirror in front of the SWIR telescope provides cross-track pointing.

The TIR optics consist of a Newtonian-mirror system with a 280-mm diameter aperture. The system is a whiskbroom scanner using an oscillating flat mirror in front of the telescope for cross-track sampling. The focal plane is populated with ten-element, small-scale linear detectors for each of the five bands.

Manuscript received November 4, 1997; revised March 9, 1998.

K. Thome, P. Slater, and E. Zalewski are with the Optical Sciences Center, University of Arizona, Tucson, AZ 85721-0094 USA (e-mail: kurt.thome@opt-sci.arizona.edu).

K. Arai is with the Faculty of Science Engineering, Saga University, Saga, 840 Japan.

S. Hook, H. Lang, and F. Palluconi are with the Jet Propulsion Laboratory, Pasadena, CA 91109 USA.

H. Kieffer is with the United States Geological Survey, Flagstaff, AZ 86001 USA.

T. Matsunaga and S. Tsuchida are with the Geological Survey of Japan, Tsukuba-shi, Ibaraki, 305 Japan.

A. Ono and H. Sakuma are with the National Research Laboratory of Metrology, Tsukuba-shi, Ibaraki, 305 Japan.

T. Takashima is with the Earth Observation Research Center, NASDA, Minato-ku, Tokyo, 106 Japan.

H. Tonooka is with the Ibaraki University, Hitachi-chi, Ibaraki, 316 Japan.

R. M. Welch is with the University of Alabama at Huntsville, Huntsville, AL 35807 USA.

Publisher Item Identifier S 0196-2892(98)04810-4.

TABLE I
ASTER BANDS AND RADIOMETRIC SPECIFICATIONS

Subsystem (& detector type)	Band #	FWHM bandpasses	Radiometric resolution	Quantization	1-σ calibration uncertainty
VNIR (Si-CCD 5000 × 4)	1	0.52-0.60	0.5%	8 bit	±4%
	2	0.62-0.69			
	3N	0.76-0.86			
SWIR (Cooled PtSi 2048 × 6)	4	1.60-1.70	0.5%	8 bit	±4%
	5	2.145-2.185	1.3%		
	6	2.185-2.225	1.3%		
	7	2.235-2.285	1.3%		
	8	2.295-2.365	1.0%		
	9	2.360-2.430	1.3%		
TIR (Cooled HgCdTe PC 10×5)	10	8.125-8.475	0.3 K	12 bit	3 K (200-024 K)
	11	8.475-8.825			2 K (240-270 K)
	12	8.925-9.275			1 K (270-340 K)
	13	10.25-10.95			2 K (340-370 K)
	14	10.95-11.65			

The detectors are mercury-cadmium-telluride photoconductive detectors located parallel to the along-track direction. The spectral bands are defined by interference filters just in front of the individual detectors. A mechanical chopper is inserted at the primary focal plane during the reverse scan of the mirror to provide ac output signals. The temperature of the mechanical chopper is monitored, as are the optical barrel, mirrors, relay lenses, etc., to compensate for the temperature drift of the offset. The cross-track pointing is obtained by rotating the whole scanning unit.

A critical component to the success of ASTER, and OES, is accurate radiometric calibration [4]. The radiometric calibration requirements of the VNIR and SWIR subsystems of ASTER are shown in Table I. The calibration techniques used for ASTER include preflight characterization of the sensor, onboard calibrators (OBC's), and vicarious methods using terrestrial sites and the moon. This paper describes the different methods that will be, or have been, used to determine the radiometric and geometric calibration of ASTER. Also, one of the key issues for determining the radiometric calibration as a function of time for ASTER will be combining the results of these different methods. A proposed method for doing this is also described.

The final topic covered in this work is that of validation. Validation is considered by some to be "calibration" of the data products. That is, the algorithms that will be used to convert the measured spectral radiance to physical properties, such as surface emissivity and reflectance will be evaluated for their accuracy. The data products for ASTER to be validated are surface radiance, surface reflectance and emissivity, surface temperature, digital elevation model (DEM) output, and polar surface and cloud classification. In addition, the at-sensor radiances and the geometric correction for the data will be validated, but in this work, we refer to this type of validation as calibration.

II. PREFLIGHT RADIOMETRIC CALIBRATION

A. Solar Reflective

The preflight calibration method used for the solar reflective range is described by Ono and Sakuma [11]. The primary standards are fixed-point blackbodies made of copper, silver, zinc, lead, and tin for the VNIR and SWIR, selected to match expected inflight radiance levels. However, their strong spectral nature requires accurate spectral knowledge of the radiometer being calibrated. The radiance of the fixed-point blackbodies were transferred to variable-temperature blackbody furnaces, where the temperature ranged from 1073 to 1723 K for the VNIR and from 323 to 723 K for the SWIR. This was done using a spectral radiance meter that included a switching mirror to select a target, double-grating monochromator and photodetectors. The spectral radiances of these furnaces were transferred to the working standard, a large spherical integrating source of 1-m diameter coated with barium sulfate and having a 280-mm aperture diameter, with 12 halogen lamps operated at dc voltage [12].

The primary uncertainty of the spectral radiance meter is due to wavelength uncertainty, with nonuniformities in the spherical integrating source also being significant. In transferring the sphere-based calibration to the OBC's, there

are additional uncertainties due to fluctuations in the output of the halogen lamps used for the OBC's. Also, air-to-vacuum shifts in the output of the onboard lamps not being cooled by convection when operated in a vacuum are expected to add to the uncertainty [4]. The total uncertainty of the preflight calibration in the VNIR and SWIR is estimated to be in the 2–3% range [4].

B. Thermal Infrared

The preflight calibration for the TIR was conducted in a thermal-vacuum chamber against a laboratory standard blackbody whose temperature was varied from 200 to 340 K. The emissivity of the standard blackbody should be better than 0.998. The temperatures of the standard blackbody were monitored by platinum resistance thermometers traceable to National Research Laboratory of Metrology (NRLM), Tsukubashi, Ibaraki, Japan. The temperature difference between the thermometer and the radiative surface of the blackbody was determined to better than 0.2 K [13]. The preflight calibration of the TIR consisted of changing the temperatures of the onboard blackbody, the pointing mirror, choppers, and other mirrors as well as the standard blackbody temperature. The results of the preflight calibration for all three subsystems are currently being evaluated, but preliminary indications are that the systems appear to behave well with all forms of noise below the digitization level.

C. Cross-Calibration Experiment in the VNIR and SWIR

An important aspect of the preflight calibration of several of the EOS sensors is the cross comparison of the calibration sources. The radiometers used for this work were several ultra-stable radiometers [14]–[16] that measured the sources used for the calibration of ASTER, MISR, and MODIS as well as other sensors from the OES. Biases seen between the outputs of the various sources will be used to diagnose and reconcile differences between inflight calibrations and cross comparisons.

For the ASTER sources, a round-robin experiment was held February 20–23, 1995, using the VNIR spherical integrating source [17]. Groups from the NRLM, the University of Arizona, Tucson, National Institute of Standards and Technology, Gaithersburg, MD, and Goddard Space Flight Center, Greenbelt, MD, participated. A total of four radiance levels were measured by each of the four participants in the round-robin exercise. Results indicate that the spectral radiance of the ASTER VNIR source may be underestimated by 1.5% [17]. The standard deviation of the radiances from all four radiometers was only 1%, thus, this 1.5% underestimation could be significant. However, this underestimation is still within the requirements for the knowledge of the sphere's radiance. Since the specification for the calibration of ASTER for the VNIR is 4%, $\pm 1\sigma$, the results are well within the uncertainties and are quite encouraging, considering that the experiment used four radiometers, designed, built, and calibrated independently to the standards of two different national laboratories. Results from a similar experiment, held more recently, that included measurements in the SWIR are still being evaluated.

III. Preflight Geometric Calibration

The goal of the geometric calibration is to achieve pixel geolocation accuracy of 100 m at nadir, with an intratelescope registration of 0.2 pixels and an intertelescope registration of 0.3 pixels. During the subsystem preflight tests, the line-of-sight vectors were evaluated against the boresight coordinate frame of each telescope using a collimator. Since the boresight coordinate frame changes, depending on the cross-track pointing position, a coordinate transformation identifies the line-of-sight vectors for an arbitrary pointing position. These line-of-sight vectors were evaluated against the body-fixed coordinate system of each subsystem at the initial stage of preflight geometric calibration. The average boresight vector for each telescope is defined as the boresight coordinate frame for the nadir pointing position. For the SWIR and TIR telescopes, the stagger configuration of detectors is taken into account by aligning to the center position. During the integration and test on the spacecraft, the nadir boresight coordinates for each subsystem are aligned to the spacecraft reference axes, except for TIR subsystem, which is rotated by 0.3°. For the VNIR subsystem, the boresight coordinates will be represented by the nadir telescope.

IV. Inflight Radiometric Calibration

A. OBC Description

The OBC for the VNIR consists of two identical optical trains made from a folding mirror and other optical elements that direct light from a tungsten-halogen lamp through a small portion of the aperture onto the focal plane. A photodetector monitors the output from the lamp and an additional photodetector monitors the output of the OBC on the focal plane. The SWIR OBC is similar with two identical system calibrators based on lamp sources. The light from the lamp sources are directed to the focal plane via the SWIR pointing mirror, thus checking the full optical path. The lack of optical elements in the SWIR calibrator means that only one photodector is needed to monitor the output from each lamp. The total uncertainty for the radiometric calibration using the OBC's is estimated at 3.8% [4].

The OBC for the TIR optical system uses a flatplate, honeycomb surface as a blackbody designed to have an emissivity greater than 0.99 [18], [19]. The pointing mirror of the TIR subsystem directs the blackbody output onto the sensor. The blackbody temperature is monitored by platinum resistance thermometers, and the temperature is controlled by radiative cooling. In order to calibrate the system at multiple temperature levels, the blackbody is heated to 340 K using point electric heaters once every 16 days. The output of the blackbody is monitored during the 35 min needed to heat it, and cool down from this 340-K temperature back to the 270-K normal operation takes approximately 4 h [19].

B. Ground-Referenced Methods

The term "ground-referenced methods" refers to vicarious calibration approaches that rely on ground-based test sites, including both land and water targets. The methods that will

be used for ASTER in the solar reflective are the reflectance-based, irradiance-based, and radiance-based methods. The TIR will use the radiance-based and temperature-based approaches. Cross-calibration techniques will be used for all three subsystems.

The reflectance-based approach relies on ground-based, surface reflectance measurements of a selected target at the time of sensor overpass [20], determined by ratioing radiometer measurements of the site to those of a panel calibrated in the laboratory [21]. Atmospheric measurements of solar extinction and sky radiance are made at the same time, and these are inverted to obtain aerosol size distribution and columnar ozone [22]. The results of the surface and atmospheric measurements are used as input to a radiative transfer code to predict the top-of-the-atmosphere (TOA) radiance [23]. We compare the average of the digital numbers of the selected site as reported by the sensor to these predicted radiances to give the radiometric calibration.

The reflectance-based approach relies on numerous assumptions about the size and composition of aerosols in the atmosphere, and incorrect assumptions lead to errors in the computed radiance at the TOA. The irradiance-based approach was developed to reduce the problems of some of these assumptions [24]. This method uses measurements of the downwelling, global, and diffuse irradiances to determine the radiance at the TOA. The irradiance-based method will be applied to the calibration of the VNIR bands of ASTER and should allow us to determine if there is a bias between the reflectance- and irradiance-based methods.

In the radiance-based approach, the radiometer measurements of the upwelling energy from the test site are no longer ratioed to measurements of a field-reference panel [20]. Rather, the field radiometer is absolutely calibrated in the laboratory, and the upwelling radiance from the test site is determined directly from the measurements. Because no reference-panel measurements are needed, the radiometer can be flown in an aircraft and the radiance can be measured above much of the scattering influences of the atmosphere. This reduces uncertainties due to the atmosphere that are present in the reflectance- and irradiance-based approaches. An additional advantage to flying the radiometer is that a much larger test site can be measured in a short period of time. This method will be applied to all three subsystems of the ASTER sensor.

Nonimaging radiometers are typically used for the radiance-based approach because they are usually easier to characterize radiometrically due to their straightforward design, low number of moving parts, and small number of detectors. Thus, the test sites for this method have to be uniform enough so that misregistration between the aircraft and ASTER data is not a large source of error. This problem is partially avoided by using a boresighted video system to help determine where the airborne radiometer is looking at a given time. Another difficulty with the radiance-based approach is the fact that the satellite's angular field-of-view and the airborne radiometer's field-of-view will be quite different. This causes uncertainties due to bidirectional reflectance effects and also registration. All of these effects are reduced by selecting a site that is spatially and spectrally uniform and nearly Lambertian.

The temperature-based approach for the TIR bands uses measurements at the time of sensor overpass of the surface temperature of the test site. When coupled with the spectral emissivity in a radiative transfer code, the radiance at the sensor can be predicted in a similar fashion as the reflectance-based approach. Atmospheric characterization is required here as well, except now the radiative processes are dominated by the vertical profile of temperature and humidity rather than the scattering properties of the atmosphere. This profile information is typically obtained through radiosonde launches near in time to the satellite overpass and spatially close to the test site.

Because the measurements required for these vicarious methods are similar in nature, several of the methods will be applied to the same ASTER scene. This has the advantage of offering multiple, independent calibrations for the same field campaign as well as allowing for validation of ASTER data products, such as the atmospheric correction.

In addition to the three vicarious methods just described, we will use inflight, cross-calibration techniques to transfer the calibrations of ASTER, Land Remote-Sensing Satellite (Landsat)–7 Enhanced Thematic Mapper (ETM)+, Multiangle Imaging SpectroRadiometer (MISR), and Moderate Resolution Imaging Radiometer (MODIS). The approach is identical to the radiance-based approach, except the well-calibrated radiometer is a satellite-based system rather than an airborne sensor. A similar approach can be used with airborne radiometer, such as the Airborne Visible and Infrared Spectrometer (AVIRIS). The method is easiest to apply when both sensors are on the same platform, reducing effects due to surface bidirectional reflectance factor (BRF), atmospheric conditions, and sensor-to-sensor registration. This is the case with ASTER, MISR, and MODIS on the EOS-AM1 platform. Larger uncertainties occur when sensors are on separate platforms, as with Landsat-7, where it is necessary to correct for changing atmospheric conditions and bidirectional reflectance distribution function (BRDF) effects. The cross-calibration method will be implemented in two fashions. The first includes ground-based measurements at the times of the overpasses. The second approach does not include ground-based data. This allows for a larger number of calibrations, but the larger uncertainties must be understood before the results are used to determine the radiometric calibration.

To better understand the feasibility of cross calibration of satellite sensors, we used data from Landsat-5 Thematic Mapper (TM) and Systeme Pour l'Observation de la Terre (SPOT)-3 Haute Resoluté Visible (HRV) of White Sands, NM, on October 8 and 9, 1994, respectively [25]. The atmospheric conditions on both days were measured, as was the surface reflectance of the test site. These data were used to determine reflectance-based calibrations of both sensors. The cross calibration used bands 2–4 of TM matched with bands 1–3 of HRV, respectively. For each pair of bands, the spectral responses were used to determine spectral corrections between bands from ground-based spectral reflectance data. To account for pixel size differences, each pixel for both sensors was divided to create 10×10-m pixels and the images were registered using ground control points (GCP's). The near-

Lambertian quality of the site and similar view/solar geometry resulted in less than a 0.1% change in the reflectance due to BRF effects. Results showed it is possible to retrieve the calibration coefficient of TM, using HRV, to <1% of the reflectance-based values when band-to-band differences in the spectral reflectance are taken into account [25].

Cross calibration is also planned for the TIR using ASTER, ETM+, and MODIS to allow us to determine biases between the three systems. Our intent in the TIR is not to perform an accurate absolute calibration, but rather a precise relative calibration to determine if there are any problems with the onboard blackbodies. For ASTER and MODIS, the largest uncertainties will be from spectral differences in the bands due to spectral emissivity and atmospheric effects. For the cross calibration of ETM+, we will also have to consider temporal changes in the surface temperature of the test site and atmospheric changes. Using a large water target, such as Lake Tahoe, CA, should reduce the emissivity and temporal effects.

Critical to the vicarious methods is the test sites. Currently, the primary site for VNIR and SWIR small-footprint sensors is part of the alkali-flats area of White Sands Missile Range. Fig. 1 shows spectra retrieved from White Sands. From this figure, it is clear that White Sands has high reflectance in the blue portion of the spectrum. Unfortunately, it also has much lower, spectrally-varying reflectance in the SWIR. The numerous SWIR bands of ASTER prompted us to consider additional sites, such as Lunar Lake and Railroad Valley Playa, two dry lakebeds in central Nevada. Spectra from these sites are also shown in the figure. Other effects to consider, in addition to spectral reflectance, are spatial uniformity, size, BRF, and temporal variability. Of the sites we have already used, Lunar Lake is the most uniform, but unfortunately it is the smallest, causing problems for cross calibration with larger footprint sensors, such as MISR and MODIS. The small size of Lunar Lake may also cause problems due to atmospheric adjacency effects. Preliminary studies indicate White Sands should be spatially uniform enough for cross-calibration work with large-footprint sensors [26], but the poor reflectance in the SWIR shows the need for additional sites. All of these sites vary throughout the year depending on seasonal rainfall, and this must be taken into account when both selecting a site and when selecting a time of year to collect data at a site.

For the TIR, the planned sites are large lakes because water has the advantage that the spectral emissivity is essentially known and temporal changes in surface temperature are relatively small over the period of the measurements. However, spatial homogeneity is still an issue. One proposed site for ASTER is Lake Tahoe. This target is large enough that it is suitable for both the temperature-based approach and cross-calibration methods.

B. Lunar Calibration

A recent change in the mission planning for the EOS-AM1 platform includes an opportunity for ASTER to view the moon through an attitude maneuver that sweeps the platform "nadir" direction through deep space and past the moon. The baseline

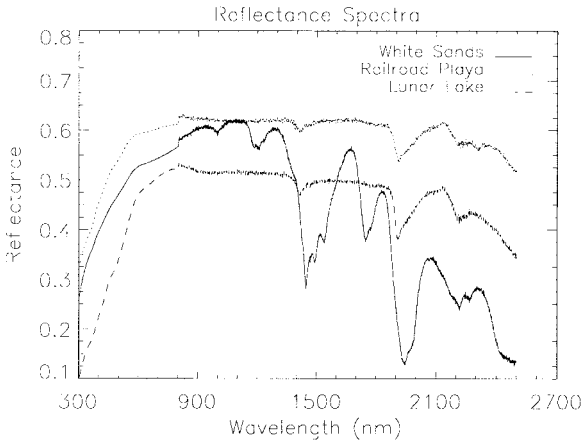

Fig. 1. Results of spectral reflectance measurements of vicarious calibration site samples.

maneuver is a pure pitch maneuver, with the moon imaged at a phase angle near 22°. The maneuvers are expected to occur early in the mission as well as once or twice a year during the mission. The apparent size of the moon is 6.4 km in the cross-track direction, with the downtrack extent depending upon the pitch rate of the platform. This means that the lunar image will subtend about 427 pixels in the VNIR, 213 pixels in the SWIR, and 71 pixels in the TIR.

The moon can be used in several ways to support the calibration of ASTER. Although lunar irradiance varies greatly with phase angle through a month, and mildly, with libration, changes in the intrinsic photometric stability of the lunar surface are estimated to be less than one part per million per year [27]. Thus, a view of the moon early in the mission lifetime can be compared to one later in the mission to determine the sensor degradation and long-term drift. Comparisons with views of the moon obtained by other EOS and non-EOS sensors can be used to determine relative gains between sensors. A lunar maneuver also provides the TIR subsystem of ASTER a view of deep space for a key point on the responsivity curve. Finally, the lunar maneuver provides an absolute radiometric source and a source to study the instrumental modulation transfer function (MTF).

The absolute radiometric calibration of the VNIR and SWIR bands of ASTER will be done using the results of a project currently underway as part of OES to develop a lunar radiance model. This model will allow the radiance of the moon to be determined as a function of the earth–moon geometry for the VNIR and SWIR portion of the spectrum [27]. The results of the model are expected to have an uncertainty less than 2%.

One possible effect in the lunar calibration that may need correction is that due to the small apparent size of the lunar disk relative to the laboratory sources and terrestrial targets used for the calibration of the sensor. This smaller size can lead to differences in the results due to the different out-of-field and stray-light radiance distributions. The correction can be determined by treating the lunar data as a simple scattered-light analysis of a bright object surrounded by virtually zero background radiance. The ASTER data can be averaged in the along track to correct for the scan rate yielding a conformal

image. This image is virtually a scattered-light response map to a 0.5° diameter source. Combining the line spread function described below and the scattered light analysis, allows a two-dimensional (2-D) response function of ASTER to be approximated. This function can be integrated radially from the center of the instantaneous field-of-view (IFOV) to generate the "encircled energy response," or size-of-source, function out to an angle equivalent to the angular distance from the edge of the moon to the edge of the lunar scene, expected to be about 1.5°. Response beyond this angle should be very small for all ASTER bands. Determination of far-off-axis scattered-light sensitivity in flight is difficult, and no method has been formally identified.

The view of a high-contrast target with low-radiance background also allows for studies of the sensor MTF. The initial assumption will be that all detectors in a band have the same MTF. The bright limb of the moon can be treated as a "knife-edge," allowing a line spread function to be determined. The cross-track, line spread function determined in this manner is directly applicable to the instrument. The along-track value requires correction for the unusually slow motion of the image. If it is assumed that attitude jitter during the lunar observations is representative of that during nadir observations, the derived line spread function represents the effective spatial resolution of ASTER data.

C. Geometric Calibration

Geometric calibration determines the detailed spatial response of each ASTER band, with respect to the nominal telescope pointing direction. This includes both the "central" directions of each pixel and the shape of the response function of individual pixels. Determining the detailed spatial response function is a necessary companion to absolute radiometric calibration because response outside the central region containing the nominal IFOV may be comparable to, or greater than, other uncertainties of radiometric calibration using sources considerably larger than an IFOV. Preflight measurements of the line-of-sight vectors for each of the telescopes may not be sufficiently accurate for precise band-to-band registration. Real image data are essential for precise registration, but it was not possible to have focused image data during the preflight test activity on the ground. The absence of geometric calibration tests after payload integration on the EOS-AM1 platform means that the possible influence of other instruments (e.g., vibration) will not be determined. In addition, the simple act of launching the platform may make the preflight data unsuitable. Therefore, inflight image data are necessary for the preparation of the geometric database for operational use. This inflight geometric calibration will be carried out during the early checkout period scheduled for the first 105 days after launch. The initial checkout activity for the geometric database consists of three parts; an intratelescope registration error correction, intertelescope registration error correction, and a geolocation error correction.

The intratelescope registration applies image-matching techniques to each telescope using a band near the center of each telescope's focal plane as the reference. For the VNIR, this is band 2, band 4 for the SWIR, and band 11 for the TIR. The correlation windows are 42 $\times$ 42 pixels for VNIR, 21 $\times$ 21 pixels in the SWIR, and 7 $\times$ 7 TIR pixels. For the SWIR, a parallax correction is calculated from elevation information of the scene and subtracted from the image-matching error in the along-track direction to evaluate alignment error. The line-of-sight errors for roll, pitch, and yaw components of each band are derived from analysis of x–y offsets of detectors spaced across the scene and stored in an off-line database. The vectors for other detectors are evaluated from linear interpolation. This intratelescope registration correction will only be done during the initial checkout period because the within-telescope-detector alignment should be stable, specified to be $<$0.2 pixels during the life of the instrument.

The intertelescope registration uses band 6 of the SWIR and band 11 of the TIR relative to the reference, band 2. The parallax error between these bands is small, thus, the scenes used for intertelescope registration need not be the same scenes used for intratelescope registration. Subscenes of the same size as used in the intratelescope registration are used here. The scenes are matched in both the along-track and the cross-track directions with subpixel resampling when necessary. The difference in registration between the pixel nearest the center of each subscene is used to determine the correction. The corrections determined for bands 6 and 11 are applied to all other SWIR and TIR bands. This correction is split into static and dynamic components, with only the dynamic part corrected by image matching during the normal operation phase.

The geolocation error detection is determined only for band 2, with the accuracy for other bands determined through the intrabands and interbands registration processes. Therefore, the scenes of VNIR band 2 that include specially prepared GCP chips for the validation of geolocation are selected. A special GCP file is being prepared using the 18-m data from Japanese Earth Resources Satellite (JERS)-1 and 10-m SPOT panchromatic data. Roughly 30 scenes with 10–20 GCP's each will be prepared throughout the world to evaluate the static pointing error, including possible periodic variation through a spacecraft revolution around the earth. Both standard and high-accuracy GCP's are being defined. The standard GCP's are known to an accuracy of better than 15 m in X and Y and 50 m in Z. Approximately 300 of these points will be compiled for the initial checkout activity. The high-accuracy GCP's are known to better than 1.5 m in X and Y and 2.5 m in Z. A list of 20–30 of these points will be compiled for the initial checkout activity. In collaboration with Landsat-7 and the United States Geological Survey, Flagstaff, AZ, dense sets of GCP's are being established at two sites where extensive digital orthophotographic map coverage will be available by late 1998. These GCP files will correspond to 185-km wide strips of Landsat scenes with 600-km length.

Inflight geometric calibration will also include high-contrast test sites to evaluate the MTF. Ideally, the test site should be of two uniform and known brightness levels for which the geometry is well known, such as resolution bar targets. No such ideal targets are known of spatial scales appropriate for ASTER, but large bridges over water provide data for

a calculation of line spread function. Parallel roads are also good targets. Since the resolutions of each subsystem are different, the targets will be selected for each sensor system. One difficulty with this approach is accurately correcting for atmospheric effects.

V. Use of Calibration Results

ASTER will be calibrated using the multiple methods described previously. These multiple calibration inputs will, however, introduce the problem of how to combine results in a reliable manner to provide the best absolute calibration as a function of time over the mission lifetime. Previous approaches include the method proposed for SPOT HRV that has the advantage of combining the absolute accuracy of the vicarious calibration with the high precision of the OBC [28]. Slater and Biggar [29] review several other proposed methods for combining the various sources of calibration coefficients. The approach proposed for MISR uses an unweighted average of the onboard and vicarious calibrations in an automated procedure that will operate online at the MISR Science Computing Facility [30]. A Kalman-filter approach has been proposed for combining the three sources of calibration (solar diffuser, partial aperture calibrator, and ground-reference methods) expected for Landsat-7 ETM+ [31].

For ASTER, one approach considered was to use the OBC data alone to generate the coefficients needed to radiometrically correct ASTER data. A second set of coefficients would be developed to merge the vicarious results with the OBC results after review by a panel of ASTER Science Team members. This panel will determine the weighting to assign to each of the calibration data sets, and the refined set of coefficients will be made available to the science community. This has the advantage of providing a timely data product for users, but unfortunately does not provide what could be the best possible radiometric product.

An alternate approach is to use the vicarious results to indicate when the accuracy of the OBC data has degraded to a level that it needs to be adjusted. When this threshold is reached, the OBC data are forced to match the results of the vicarious calibration. The overall trend of the calibration is still determined from the OBC data because of its higher temporal resolution. This approach takes advantage of the high-precision and temporal sampling of the OBC data, while using the accuracy of the vicarious methods. The disadvantage to this approach is determining the threshold at which to adjust the calibration coefficients. If the threshold is too high, adjustments in the calibration coefficients as a function of time have a large step function that will show up as an artifact in mosaics of multiple images. If the threshold is too low, the calibration coefficients will be altered so often as to burden the processing of the ASTER data. Both approaches are currently being developed, with plans to select a final method after the data from the initial checkout period are evaluated.

VI. Validation Plan for ASTER

The EOS project has developed a set of terminology to refer to data products. The raw data are referred to as Level 0 data. Level-1A data are the reconstructed, unprocessed instrument data at full-resolution, time-referenced, and annotated with ancillary information, including radiometric calibration and geometric correction coefficients and georeferencing parameters computed and appended, but not applied to the Level-0 data. The Level-1B data are the Level-1A data processed using the radiometric calibration and geometric correction coefficients to registered radiance at sensor. This step typically involves irreversible resampling. The Level 1B data are typically used as input to the higher level data products. Level-2 data are the results from the various algorithms that take the Level-1 radiances and convert them to physical quantities. Level-3 data are Level-2 data that have been further processed by either reformatting or deriving an additional physical property from the Level-2 results. Two examples of Level-3 data would be a composite of Level-2 surface reflectances for the continental United States or deriving a surface classification based on the Level-2 surface emissivity. In this work, we discuss the validation of ASTER Level-2 data only.

A. Surface Radiance and Reflectance in the VNIR and SWIR

The algorithm to derive the surface reflectance and radiance in the VNIR and SWIR has been previously described [32]. The validation approach for this algorithm is similar to past work [33] and is based on the methods developed for the reflectance-based calibration. The reflectance of a selected target is determined by transporting spectroradiometers across a selected test site to measure the upwelling radiance. These data are converted to reflectance by reference to a panel of known reflectance. The measured surface reflectance and radiances are then compared to those derived from the standard processing of the ASTER data. In addition, solar radiometer and sky radiance measurements at the site are used to determine the aerosol properties and columnar absorber amounts over the site [22], [34], [35]. The atmospheric measurements made at the site at the time of sensor overpass will be used as inputs to the processing to determine the effects of input uncertainties.

The above measurements provide an opportunity to validate both the inputs to the atmospheric correction and the output products. This is important because it is expected that input uncertainties will dominate the overall uncertainty. Additionally, determining input uncertainty effects should allow for a reduction in the number of field campaigns required to validate this product by allowing the ASTER team to focus experimental, validation efforts on those cases expected to show where there are problems in the algorithm. For example, studies show that the radiance at the sensor from high-reflectance targets has relatively little sensitivity to aerosol optical depth for optical depths less than 0.2. This would not be a high-priority case to validate because large uncertainties would not be expected for this situation.

The most difficult aspect of this validation effort is test-site selection. To completely validate this product would require test sites satisfying a wide range of surface reflectances, surface relief, horizontally varying surface reflectance, different aerosol types, a range of aerosol concentrations, and varying

amounts of absorbing gases. If only the extremes are selected, this leads to validation sites that have combinations of low- and high-aerosol optical depths, two different aerosol types (marine and continental, for example), low and high humidities, dark and bright surfaces, flat and highly sloped surfaces, horizontally a homogeneous surface and one with widely varying reflectance, and clear and thin-cloud cases. This would require a large validation budget. Thus, a compromise is required to select targets that first ensure the algorithm operates properly for simplistic cases. Then theoretical data are used to predict cases in which the algorithm might have difficulties, and we select targets to evaluate these predicted problem areas [36].

For the simplistic case, the site must be large enough and homogeneous enough so that the average reflectance of a "pure" ASTER SWIR pixel can be determined and should have several areas that are at least 45×45 m in size with spatially uniform reflectance. The target area should have moderate levels of turbidity (aerosol optical depths >0.30) and preferably a possibility of both continental and marine aerosols. Ideally, the site has high probability of cloudless skies to increase the chance of successful field campaigns and easy access. Proximity to ASTER team members helps to reduce travel costs, and current plans are to use the Los Angeles, CA, basin and an area north of Tokyo, near Tsukuba, Japan. Once the algorithm is validated for the "simple" case of a large homogeneous target, other sites will be used based upon radiative transfer code results indicating desired characteristics of such sites.

B. Surface Radiance in the TIR

The TIR surface radiance product is the surface-leaving spectral radiance in the five ASTER TIR channels. This radiance is a combination of direct emission by the surface and reflection of radiation incident on the surface from the surroundings, including sky radiation. Validation of the retrieved surface radiance will rely on field experiments similar in philosophy to the validation of the atmospheric correction of the VNIR and SWIR bands. The experiments rely on water targets, such as Lake Tahoe and the Salton Sea, that provide a range of atmospheric conditions (e.g., warm surface and humid atmosphere, warm surface and dry atmosphere, cold-humid, and cold-dry). Water targets are preferred over land targets due to their high thermal inertia. Land targets are also being investigated to understand problems associated with limited sampling in space and time and to take advantage of the high temperatures (>300 K) that land surfaces can provide.

The validation approach compares surface radiance reported by the atmospheric correction algorithm to that derived from measured surface kinetic temperature, the ASTER spectral response, surface emissivity, and sky irradiance. The kinetic temperature is measured at the surface over several ASTER TIR pixels. In addition, for water targets, an array of continuously recording buoys is used to estimate the space and time variation in water temperature. To reduce geolocation error, 3×3 pixel areas will be instrumented and their location determined relative to the shoreline. Radiosonde profile measurements are used to determine the atmospheric temperature and moisture profiles for use with the radiation model Moderate Resolution Atmospheric Radiance and Transmittance (MODTRAN) to estimate the spectral sky irradiance.

C. Surface Kinetic Temperature and Surface Emissivity

The Temperature/Emissivity Separation (TES) algorithm generates the surface temperature and emissivity product that is an elaboration of the earlier normalized emissivity and the alpha-derived emissivity methods [38]. The validation of both the temperature and the emissivity is described together because they are closely interrelated and must be calculated with a single algorithm. Although the earth's surface is complex, the TES validation will consider only two types of scenes: 1) those of near-graybodies for which the spectral emissivities are known and homogeneous, and the surface temperatures are known or homogeneous and can be readily measured during overflight, and 2) "colored" surfaces for which emissivity spectra depart from graybody values but are homogeneous. The first instance corresponds to the important class of scenes covering bodies of water, ice sheets, snow fields, and closed-canopy vegetation. The water and snow scenes will also coincide with targets used for the validation of the surface radiance product. For these scenes, the primary goal is to recover surface temperature since the emissivities are closely known in advance. The second instance corresponds to the class of scenes for which soil and rock are exposed. Surface temperatures cannot be recovered unless emissivities are recovered also, since they are not known in advance. This type of scene is common in the arid third of the land surface.

The temperature and emissivity standard products will be validated by comparing TES values with simultaneous measurements made 1) in the field by ground instruments, 2) airborne scanners, such as Thermal Infrared Multi-Spectral Scanner (TIMS), MODIS/ASTER Airborne Simulator (MASTER), and MODIS Airborne Simulator (MAS), and 3) MODIS. For the "colored" surfaces, the main problem is to measure representative scene emissivities and to assess spatial heterogeneity, so that the validation data can be correlated to the appropriate ASTER pixels. Several hundred spectra will be measured until the emissivity at the 90-m scale, estimated from the 10-cm-scale field measurements, is felt to be well determined. Once these are established it is not necessary to measure them again. Thus, during ASTER, it is sufficient to measure surface temperatures and atmospheric characteristics, as is done in the case of the atmospheric correction validation.

D. Polar Surface and Cloud Classification

The overriding objective of the ASTER Polar Cloud Mask product is to identify or classify all pixels in imagery obtained poleward of 60° latitude as cloud or clear. Depending on the type of user, the product can be used to mask out all cloudy pixels for surface studies (e.g., ice process studies) or, conversely, all clear pixels for polar cloud studies. The validation of this product is based on techniques learned while validating the algorithm's application to Landsat TM.

One method used in the validation is by application to a labeled set of samples. To date, approximately 3700 contigu-

ous pixel regions (made up of several hundred thousand pixel samples) have been extracted and labeled by a human expert trained in identifying features in polar imagery. For every pixel in every contiguous sample, the classification results from the algorithm are compared to the labeling (test samples) and a "confusion" matrix is generated, indicating the percentage of classification for each combination. If the algorithm performs perfectly, the confusion matrix is diagonal and each diagonal element is 100%. This method somewhat overestimates the algorithm's accuracy because the human expert tends to select spectrally homogeneous and unambiguous samples that are generally classified at a higher accuracy rate. However, this approach provides an indication of the upper limit of performance and will serve as the basis for validating the accuracy of the algorithm over the life of the product.

A second validation approach is more objective and involves visual comparison of the classification result with the imagery by a human expert. The expert has access to tools, allowing him to augment his analysis using three-band overlays and other image processing techniques, such as contrast stretching and histogram equalization. More than one expert is typically used, and their estimates of the accuracy are generally within 5% of each other.

A final image-analysis approach is an attempt to quantify the overall scene classification accuracy. This is derived from a tool that a human expert uses to label randomly selected regions within the imagery. It is very much like the process that an expert uses to extract labeled samples, except the computer randomly selects the region to be labeled as opposed to the expert selecting the region. The random selection of samples by the computer provides a more objective estimate of classification accuracy when these samples are compared against the results obtained from the classifier.

The results obtained from these methods will also be compared with independent observations from ground-, air-, and other satellite-based observations. Comparisons with these other types of observations will be conducted over an extended period of time for a variety of circumpolar regions. The validation effort for this algorithm will take advantage of any data obtained from field studies conducted prelaunch and postlaunch in which polar-like conditions are present. The validation effort using surface observations will also take advantage of the enhanced surface-based measurement capabilities located at the Department of Energy (DoE) Atmospheric Radiation Measurement (ARM) sites in Alaska and Oklahoma. The use of the ARM site data from Oklahoma will be limited to wintertime conditions, especially when snow and clouds are present during the time of overpass. An opportunity for validating the algorithm in the detection of thin cirrus will also occur during overpasses of Salt Lake City, UT, using the long-range lidar and radar observations.

E. Digital Elevation Models

The shape of the surface of the planet earth (topography of the land and bathymetry of the oceans) is a fundamental geophysical parameter required for quantitative research in nearly all disciplines of earth science. Land topographic data and derived measurements of slope and aspect are also required for quantitative correction of most space-acquired radiometric measurements of the land surface, including those of MODIS and ASTER. As mentioned, the ASTER instrument includes an along-track stereo imager capable of acquiring coherent, digital, cloud-free global coverage of the earth's land surface during the six-year mission. The system is configured to acquire data with a base-to-height ratio of 0.6 at 15-m spatial resolution and can acquire 50, 700 $\times$ 60-km stereo pairs per day. The specific objectives of the ASTER stereo experiment are 1) to acquire cloud-free stereo coverage of 80% of the land surface between 85° N and 85° S and 2) to produce, with commercial software, standard product DEM's at a rate of one-per-day starting at launch.

Because of the well-established nature of the DEM-generation algorithm, we will not focus on its validation [38], but rather, evaluate the uncertainties obtained from the application of this algorithm to the ASTER data. To do this, numerous validation sites have been established by the ASTER team for which there exist higher resolution DEM's from other sources. By subtracting the heights of these sites from those derived from the ASTER DEM's covering the same area, on a pixel-by-pixel basis, an rms error of the height will be calculated. The planimetric accuracy over each validation site is determined by measuring the horizontal displacements of distinct topographic features on elevation profiles derived from ASTER DEM's, with respect to the same features on the same lines of profile derived from the comparison DEM's. Also, the locations and elevations of GCP's withheld from the ASTER-DEM generation process will be compared with their locations and elevations on the DEM. Comparison of these rms errors results with the specifications will determine if the standard data product meets specifications. This validation will be performed over each validation site at least once per year in this way to monitor system stability over the six-year mission.

F. Use of Validation Results

The validation results of the Level 2 data products will be used in two fashions. The first will be simply to supply uncertainty estimates to the user community. The second is that the results of these uncertainty measurements will be used to evaluate areas where the algorithms breakdown, can be improved, or require further testing. Algorithm modifications will then be made in subsequent deliveries of the production code. Thus, the Level 2 processing will be evolving over the lifetime of the sensor as we better understand the instrument and algorithms.

VII. Results of Joint Calibration/Validation Campaigns

For the past two summers, the members of both the Japanese and United States ASTER science teams have participated in joint field campaigns to Lunar Lake and Railroad Valley Playa. These campaigns also included representatives from the Landsat-7, MISR, and MODIS science teams as well as several non-EOS investigators. The purpose of these campaigns are to determine the level of agreement between different groups

performing vicarious calibration and validation work. The first campaign was held May 30–June 4, 1996. The 1997 campaign was held June 23–28. Results of the 1996 campaign are summarized here as are preliminary results from the 1997 campaign as an example of how the fieldwork related to ASTER will be used to both understand the sensor and algorithms after launch and to improve the accuracy of the field data.

For the solar reflective work, the 1996 campaign consisted of several data collections per day at 1420, 1600, 1800, and 2120 UTC to simulate the solar zenith at the time of ASTER overpass for a variety of times during the year. The primary target was a representative 240 $\times$ 240-m area of the Lunar Lake playa, assumed to approximate 64, 30-m pixels. The Japanese and United States groups from ASTER both used a reflectance-based approach to predict the radiances. Several simulated spectral bands were used for the experiment and details on the full set of results are given by Arai *et al.* [39]. Comparisons between predicted radiances of the Japanese and United States results showed differences of 4–10% in the VNIR. Radiances were also predicted for the SWIR, but these results suffered from higher uncertainties due to equipment malfunctions. The primary cause of these differences were later found to be due to the calibration methods of the reference panels used to determine the surface reflectance, and this accounted for up to 7% of the difference.

Other sources of uncertainty include differences in aerosol optical depths, aerosol size distribution, columnar amounts of gaseous absorbers, and radiative transfer codes. Differences in predicted aerosol optical depths for each of the bands were less than 0.01, causing differences in the predicted radiances of less than 0.6%. Aerosol size distribution effects were found to be 0.7%. When both the size distribution and optical thickness differences are combined in the radiative transfer code runs, results are less than 0.5% different. Gaseous absorption had only a small effect on the radiance at the sensor and is not a significant source of difference in these results. Since two different radiative transfer codes were used, the codes are also a source of difference. The United States group relies on a Gauss–Seidel iteration code, while the Japanese group uses a doubling-adding method. To evaluate the effect of the radiative transfer codes, the inputs from each group were run as input to the other group's codes and the differences were found to be less than 1%.

In order to actually calibrate the ASTER bands, the normalized radiances that are the output of the radiative transfer codes must be converted to absolute radiances. This is done by multiplying the normalized radiances by the exo-atmospheric solar irradiance. Both the United States and Japanese groups derived values of solar spectral irradiance using MODTRAN 3.0. Even though the same source of irradiances were used, differences in band averaging the MODTRAN output still led to differences of up to 2%. These differences can be easily corrected by simply agreeing upon one single set of values to use, but this only improves the precision of the results.

Because the differences of this first experiment were larger than desired, the second campaign included measurements to better determine the sources of the differences. Since the reference panels were a primary source of differences, all of the panels were calibrated at a single facility at the University of Arizona. In addition, all reflectance measurements in the field included measurements of a "standard" reference. This allows all of the data to be processed using the same software and with reference to the same standard to determine differences due to reference panel characterization. Preliminary results from this campaign derived for ASTER bands 1 and 2 show differences in the predicted normalized radiance of 1.6 and 2.4% between the United States and Japanese groups, when both groups use the laboratory calibrations of their respective field standards. When converted to absolute radiance, the differences are 1.8 and 0.4%.

VIII. Conclusions

The preflight calibration of ASTER in the solar-reflective range provides the first case that two very different techniques, the freezing point blackbodies of NRLM and the detector-based methods of NIST, have been referred to in the calibration of the sources used to calibrate a space sensor. This reference is facilitated by the measurements of the ultra-stable, transfer radiometers. The preliminary work that is still ongoing lends confidence that the 4% goal of absolute radiometric accuracy has been met. The transfer to orbit of the preflight calibration will be achieved using the partial-aperture OBC's. Because these calibrators will be carefully monitored by independent detectors, it is anticipated that this transfer will also meet the 4% uncertainty requirement. However, after some period on orbit, the OBC's may become contaminated or may no longer monitor a representative area of the aperture. The OBC for the thermal calibration may also be suspect over time as it relies on indirect measurements of blackbody temperature and emissivity.

The vicarious calibrations will be used to determine if changes of sensor response or OBC levels occur. These vicarious calibrations will include the well-known ground-reference techniques as well as a lunar look. Vicarious calibration becomes increasingly important as flight hardware ages and will be used to determine if aging occurs and then to determine the sensor calibration. These inflight, vicarious methods will also be used to evaluate the geometric calibration of the sensor. This is especially important for a sensor, such as ASTER, where the three subsystems are located at different places on the EOS-AM1 platform. This geometric calibration will rely on high-contrast surface test sites in addition to the data from lunar views.

An additional advantage to the vicarious calibration is that the methods used for this work are very similar to those needed to validate the Level-2 products from ASTER. These validation efforts will use test sites not used for the vicarious calibration to properly evaluate the output of the algorithms. The results of these validation efforts will serve the purpose of informing the user group of the uncertainties that can be expected from these data products. In addition, the results will be used by the ASTER Science Team to determine how best to improve the algorithms to provide the best possible products.

REFERENCES

[1] H. Fujisada and A. Ono, "Overview of ASTER design concept," in *Proc. SPIE*, 1990, vol. 1490, pp. 244–268.

[2] H. Fujisada, "Overview of ASTER instrument on EOS AM-1 platform," in *Proc. SPIE*, 1994, vol. 2268, pp. 14–36.

[3] ——, "ASTER sensor system," *Jpn. J. Remote Sensing*, vol. 15, pp. 1–15, 1995.

[4] A. Ono, F. Sakuma, K. Arai, Y. Yamaguchi, H. Fujisada, P. Slater, K. Thome, F. Palluconi, and H. Kieffer, "Preflight and in-flight calibration plan for ASTER," *J. Atmos. Ocean. Tech.*, vol. 13, pp. 322–335, 1996.

[5] Y. Yamaguchi, A. B. Kahle, H. Tsu, T. Kawakami, and M. Pniel, "Overview of Advanced Spaceborne Thermal Emission and Reflection Radiometer (ASTER)," this issue, pp. 1062–1071.

[6] A. B. Kahle, F. Palluconi, S. Hook, V. J. Realmuto, and G. Bothwell, "Advanced Spaceborne Thermal Emission and Reflection Radiometer (ASTER)," *Int. J. Imaging Syst. Technol.*, vol. 3, pp. 144–151, 1991.

[7] Y. Yamaguchi, H. Tsu, and H. Fujisada, "A scientific basis of ASTER instrument design," in *Proc. SPIE*, 1993, vol. 1939, pp. 150–160.

[8] F. Takahashi, M. Hiramatsu, F. Watanabe, Y. Narimatsu, and R. Nagura, "Visible and near infrared (VNIR) subsystem and common signal processor (CSP) design status of ASTER," in *Proc. SPIE*, 1991, vol. 1490, pp. 255–268.

[9] A. Akasaka, M. Ono, Y. Sakurai, and B. Hayshida, "Short wavelength infrared (SWIR) subsystem design status of ASTER," *Proc. SPIE*, 1991, vol. 1490, pp. 269–277.

[10] Y. Aoki, H. Ohmae, and S. Kitamura, "Thermal infrared subsystem design status of ASTER," in *Proc. SPIE*, 1991, vol. 1490, pp. 278–284.

[11] A. Ono and F. Sakuma, "ASTER calibration concept," in *Proc. SPIE*, 1991, vol. 1490, pp. 285–298.

[12] N. Suzuki, Y. Narimatsu, R. Nagura, F. Sakuma, and A. Ono, "Large integrating sphere of prelaunch calibration system for Japanese earth resources satellite optical sensors," in *Proc. SPIE*, 1991, vol. 1493, pp. 48–57.

[13] P. Slater, K. Thome, K. Arai, H. Fujisada, H. Kieffer, A. Ono, F. Sakuma, F. Palluconi, and Y. Yamaguchi, "Radiometric calibration of ASTER data," *Jpn. J. Remote Sensing*, vol. 15, pp. 16–23, 1995.

[14] F. Sakuma, M. Kobayashi, and A. Ono, "ASTER round-robin radiometers for the preflight cross-calibration of EOS AM-1 instruments," in *Proc. IGARSS*, 1994, pp. 1995–1997.

[15] S. F. Biggar and P. N. Slater, "Preflight cross-calibration radiometer for EOS AM-1 platform visible and near-infrared sources," in *Proc. SPIE*, 1993, vol. 1939, pp. 243–249.

[16] B. C. Johnson, C. L. Cromer, and J. B. Fowler, "The SeaWiFS transfer radiometer," vol. 39, S. B. Hooker and E. R. Firestone, Eds. NASA Tech. Memo. 104 566, 1997.

[17] F. Sakuma, B. C. Johnson, S. F. Biggar, J. J. Butler, J. W. Cooper, M. Hiramatsu, and K. Suzuki, "EOS AM-1 preflight radiometric measurement comparison using the Advanced Spaceborne Termal Emission and Reflection radiometer (ASTER) visible and near-infrared integrating sphere," in *Proc. SPIE*, 1996, vol. 2820, pp. 184–196.

[18] A. Ono and F. Sakuma, "ASTER instrument calibration plan," in *Proc. SPIE*, 1993, vol. 1939, pp. 198–209

[19] T. Maekawa, O. Nishihara, Y. Aoki, K. Tsubosaka, and S. Kitamura, "Design challenges of ASTER in the thermal infrared spectral region," in *Proc. SPIE*, 1993, vol. 1939, pp. 176–186.

[20] P. Slater, S. F. Biggar, R. G. Holm, R. D. Jackson, Y. Mao, M. S. Moran, J. M. Palmer, and B. Yuan, "Reflectance- and radiance-based methods for the in-flight absolute calibration of multispectral sensors," *Remote Sens. Environ.*, vol. 22, pp. 11–37, 1987.

[21] S. F. Biggar, J. Labed, R. P. Santer, P. Slater, R. D. Jackson, and M. S. Moran, "Laboratory calibration of field reflectance panels," in *Proc. SPIE*, 1988, vol. 924, pp. 232–240.

[22] S. F. Biggar, D. I. Gellman, and P. Slater, "Improved evaluation of optical depth components from Langley plot data," *Remote Sens. Environ.*, vol. 32, pp. 91–101, 1990.

[23] B. M. Herman and S. R. Browning, "A numerical solution to the equation of radiative transfer," *J. Atmos. Sci.*, vol. 22, pp. 559–566, 1965.

[24] S. F. Biggar, R. P. Santer, and P. Slater, "Irradiance-based calibration of imaging sensors," in *Proc. IGARSS*, 1990, pp. 507–510.

[25] C. L. Gustafson-Bold and K. J. Thome, "Cross-calibration of two small footprint sensors," in *Proc. IGARSS*, 1996, pp. 1283–1285.

[26] K. Thome and C. Gustafson-Bold, "Proposed method for the calibration of VEGETATION using HRVIR," in *Workshop Calibration Opt. Thermal Sensors*, Toulouse, France, Sept. 18–20, 1996.

[27] H. Kieffer and W. Wildey, "Establishing the moon as a spectral standard," *J. Atmos. Ocean. Tech.*, vol. 13, pp. 360–375, 1996.

[28] D. I. Gellman, S. F. Biggar, M. C. Dinguirard, P. J. Henry, M. S. Moran, K. Thome, and P. Slater, "Review of SPOT-1 and -2 calibrations at White Sands from launch to the present," in *Proc. SPIE*, 1993, vol. 1938, pp. 118–125.

[29] P. Slater and S. F. Biggar, "Suggestions for radiometric calibration coefficient generation," *J. Atmos. Ocean. Tech.*, vol. 13, pp. 376–382, 1996.

[30] C. J. Bruegge, D. J. Diner, L. DiGirolamo, and N. L. Chrien, "Level-1B algorithm theoretical basis: Radiometric product," Jet Propul. Lab., Pasadena, CA, JPL Rep. D-11057, 1994, p. 65.

[31] E. Freedman and J. Byrne, "Combining multiple sources for radiometric calibration of Landsat 7 using a Kalman filter," in *Proc. IAPRS*, 1995, vol. 30, pt. 5W1.

[32] K. Thome, "Proposed atmospheric correction for the solar-reflective bands of the Advanced Spaceborne Thermal Emission and Reflection Radiometer," in *Proc. IGARSS*, 1994, pp. 202–204.

[33] R. G. Holm, R. D. Jackson, B. Yuan, M. S. Moran, P. Slater, and S. F. Biggar, "Surface reflectance factor retrieval from thematic mapper data," *Remote Sens. Env.*, vol. 27, pp. 47–57, 1989.

[34] D. I. Gellman, S. F. Biggar, P. Slater, and C. J. Bruegge, "Calibrated intercepts for solar radiometers used in remote sensor calibration," *Proc. SPIE*, vol. 1493, pp. 19–24, 1991.

[35] K. Thome, B. M. Herman, and J. A. Reagan, "Determination of precipitable water from solar transmission," *J. Appl. Meterol.*, vol. 31, pp. 157–165, 1992.

[36] K. Thome, "Sensitivity analysis and validation plans for the retrieval of surface reflectance from ASTER," in *Proc. SPIE.*, 1996, vol. 2820, pp. 88–96.

[37] S. Hook, A. R. Gabell, A. A. Green, and P. S. Kealy, "A comparison of techniques for extracting emissivity information from thermal infrared data for geologic studies," *Remote Sens. Environ.*, vol. 42, 1992, pp. 123–135.

[38] F. Ackerman, "Digital elevation models—Techniques and application, quality standards, development," *Int. Arch. Photogramm. Remote Sens.*, vol. 30, 1994, pp. 421–432.

[39] K. Arai, S. Tsuchida, and K. Thome, "Calibration plan and preliminary field campaign for ASTER," in *Proc. EUROPTO*, 1996, vol. 2960, pp. 256–265.

K. Thome, photograph and biography not available at the time of publication.

K. Arai, photograph and biography not available at the time of publication.

Simon Hook, photograph and biography not available at the time of publication.

H. Kieffer, photograph and biography not available at the time of publication.

Harold Lang is a Research Scientist in the Earth and Planetary Sciences Division, Jet Propulsion Laboratory, California Institute of Technology, Pasadena. His research interests include the applications of optical remote sensing and DEM data for geological studies.

Tsuneo Matsunaga, photograph and biography not available at the time of publication.

A. Ono, for a photograph and biography, see this issue, p. 1160.

F. Palluconi, photograph and biography not available at the time of publication.

H. Sakuma, photograph and biography not available at the time of publication.

P. Slater, photograph and biography not available at the time of publication.

T. Takashima, photograph and biography not available at the time of publication.

H. Tonooka, photograph and biography not available at the time of publication.

S. Tsuchida, photograph and biography not available at the time of publication.

Ronald M. Welch, photograph and biography not available at the time of publication.

E. Zalewski, photograph and biography not available at the time of publication.